catalysts

MDPI

Article

Mechanistic Investigation on Hydrocyanation of Butadiene: A DFT Study

Kaikai Liu, Shuai Zhang * and Minghan Han *

Department of Chemical Engineering, Tsinghua University, Beijing 100084, China; lkk16@mails.tsinghua.edu.cn
* Correspondence: shuai-zh@mail.tsinghua.edu.cn (S.Z.); hanmh@tsinghua.edu.cn (M.H.)

Received: 5 July 2020; Accepted: 18 July 2020; Published: 22 July 2020

Abstract: The nickel-catalyzed addition of Hydrocyanic acid (HCN) to butadiene usually leads to a mixture of the branched 2-methyl-3-butenenitrile (2M3BN) and the linear 3-pentenenitrile (3PN) with a 30:70 ratio by employing mono-dentate phosphites, while a 97% selectivity to 3PN is obtained using a 1,4-bis(diphenyphosphino)butane (dppb) ligand and $Ni(COD)_2$ (1,5-Cyclooctadiene) as catalysts. To explain this phenomenon, a reasonable mechanism of the hydrocyanation, involving the cyano (CN) migration (for 3PN) and the methylallyl rotation (for 2M3BN) pathways, is proposed. The key intermediates and the rate-determining steps in the pathways have been illustrated. The methylallyl rearrangement is the rate-determining step in the formation of 3PN while the reductive elimination governs the reaction to 2M3BN, which is subsequently isomerized to 3PN. Moreover, the opposite changes of the bite angle of the intermediates and transition states explain how the reactions proceed in two different directions.

Keywords: hydrocyanation; mechanism; DFT; 2-methyl-3-butenenitrile; 3-pentenenitrile

1. Introduction

The hydrocyanation of alkenes is one of the most important applications of homogeneous catalysis in industry [1–3]. Additionally, the DuPont process, which forms the basis of an industrial process for the manufacture of adiponitrile (ADN), is an early successful example of homogeneous catalysis application [4]. Typically, the DuPont process consists of three steps, as shown in Scheme 1. The nickel-catalyzed hydrocyanation of butadiene (BD) leads to a mixture of the branched 2-methyl-3-butenenitrile (2M3BN) and the linear 3-pentenenitrile (3PN). In the second step, the undesirable 2M3BN is catalytically isomerized to the desired 3PN, employing Lewis acid as a co-catalyst. The last step is the isomerization of 3PN to 4-pentenenitrile (4PN) and its hydrocyanation to ADN. Although the toxicity of Hydrocyanic acid (HCN) requires a special experimental setup and the excess HCN causes the deactivation of the NiL_4 catalyst (L = phosphite) [5], the excellent atom economy and the inexpensive feedstocks (BD and HCN) are still great advantages of the DuPont process in relation to its practical application.

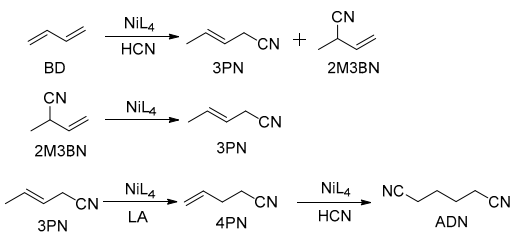

Scheme 1. The DuPont process.

The use of a nickel catalyst is intriguing due to its high effectiveness and cheapness in the DuPont process. One of the key issues is the development of new ligands to increase the catalytic activity and improve the 3PN selectivity. Originally, mono-dentate phosphites have been very popular and widely utilized, such as tri-p-tolyl phosphite and tri-m-tolyl phosphite [5,6]. In the past few years, many efforts mainly aiming to modify ligands with efficient function have been made to improve the performance of the nickel catalysts in the catalytic hydrocyanation reaction. An important step is the utilization of bidentate ligands, such as diphosphites [7], that lead to a high conversion of 2M3BN and excellent selectivity to 3PN.

Thanks to the meticulous work of Tolman [8–11], Vogt [12–15] and Jones [16–19] et al., many of the experimental variables and mechanistic aspects of the hydrocyanation reaction using a nickel-phosphite catalyst are well understood. Lewis acid (LA), such as $ZnCl_2$, BPh_3 or $AlCl_3$, is an essential co-catalyst for the rapid completion of catalytic steps (Scheme 1) [20]. Solvent effects show to be an effective tool for controlling the linear/branched ratios in the isomerization of 2M3BN [18]. Furthermore, using NiL_4 as the catalyst precursor, the reaction pathways of the hydrocyanation of butadiene have been proposed [4]. As shown in Scheme 2, one ligand L dissociates first from NiL_4 to produce the reactive intermediate NiL_3. Then, the oxidative addition of HCN affords five-coordinated cyano hydride complex A. Further, another ligand dissociation (complex B) promotes the insertion of butadiene into the nickel hydride bond, forming the methallyl complex C. From this species, subsequent reductive elimination takes place yielding the linear or branched cyano-olefin complexes D or F. Following an associative process via complexes E or G, the catalyst initializes the second catalytic cycle, releasing the branched 2M3BN and linear 3PN.

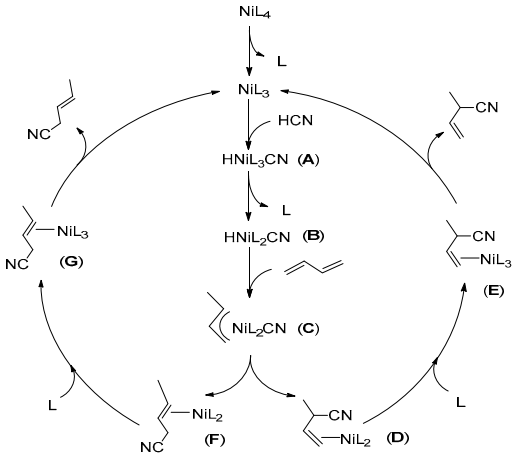

Scheme 2. Mechanism of the hydrocyanation of butadiene using NiL_4 as a catalyst.

In the isomerization of 2M3BN, there are two generally accepted mechanisms: (a) the dehydrocyanation and rehydrocyanation mechanism [20] and (b) the rearrangement via methylallyl intermediate mechanism [21] (Scheme 3). Experiments that use deuterated 2M3BN give rise to 3PN-d with statistical deuteration at C-2 and C-5 [20] and are consistent with the dehydrocyanation pathway (Scheme 3a). However, Sabo Etienne proposes the rearrangement mechanism based on the isolated Ni(η^3-1-Me-C_3H_4)(CN)(dppb) complex, (dppb: 1,4-bis(diphenyphosphino)butane) involving the following steps: (i) the coordination of 2M3BN with a nickel atom via its C=C bond, (ii) C-CN bond breaking and formation of a σ-allyl species (oxidative addition), (iii) isomerization to π-allyl species and σ-allyl formation (rearrangement), (iv) C-CN bond coupling to 3PN coordination (reductive elimination) (Scheme 3b) [21]. In addition, Density Functional Theory (DFT) calculations support that the isomerization is initiated with the C-CN bond cleavage (oxidation addition), followed by methylallyl rotation and C-CN bond reformation (reductive elimination) in the isomerization of 2M3BN to 3PN [22,23].

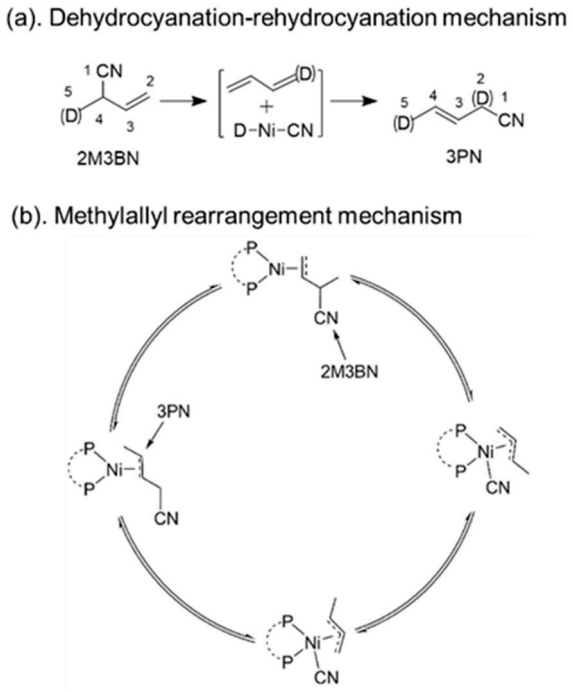

Scheme 3. Mechanism of the 2M3BN isomerization. (**a**) the dehydrocyanation and rehydrocyanation mechanism, and (D) represents deuterium. (**b**) the methylallyl rearrangement mechanism.

Recently, the unprecedented selectivity to 3PN of up to 97% has been obtained using the dppb ligand in the hydrocyanation of butadiene, which shows highly practical application and inspires us to achieve a thorough understanding by in-depth mechanistic studies. Although the mechanism for the NiL_4 catalyzed hydrocyanation [6] and the reactive pathway of the isomerization of 2M3BN to 3PN [20,21] have been reported, the hydrocyanation of butadiene employing dppb remains unknown. Therefore, the fundamental steps in the nickel-dppb catalyzed hydrocyanation process need further theoretical investigation. In this work, insight into the reaction mechanism and the comparison of different reactive pathways have been achieved by using DFT calculations.

2. Results and Discussion

The general mechanisms for Ni(dppb)-catalyzed hydrocyanation are shown in Scheme 4. The process begins with dppb-coordinated Ni(COD) complex $\mathbf{I_0}$. The other biolefin ligand COD is replaced by HCN to form the HCN-coordinated intermediate $\mathbf{I_1}$, in which the C=N group is coordinated with the Ni atom. Then, the olefin-coordinated cyano nickel hydride intermediate I_3 is generated following the oxidative addition of HCN. Subsequent olefin insertion into the Ni-H bond generates the intermediate $\mathbf{I_5}$ with a tetrahedral configuration, which is a key intermediate in the reaction pathways. Finally, the methylallyl rearrangement and C-CN bond formation by reductive elimination occurs to give intermediates $\mathbf{I_9}$ and $\mathbf{I_{13}}$, which yields 3PN and 2M3BN, respectively. Alternatively, intermediate $\mathbf{I_{13}}$ could be generated by methylallyl rotation and a different reductive elimination. With the proposed pathways in hand, DFT calculations were performed to reveal the mechanism of this nickel-catalyzed hydrocyanation.

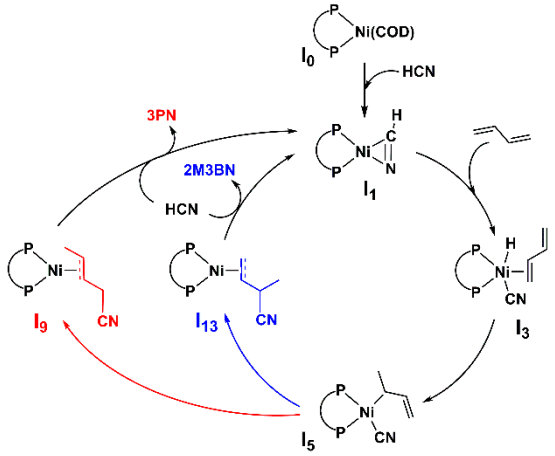

Scheme 4. Mechanism of hydrocyanation using Ni-dppb complex as catalyst.

2.1. HCN Addition and Butadiene Insertion

The free energy profiles (ΔG (kcal/mol)) for the initial steps of this nickel-catalyzed hydrocyanation are shown in Scheme 5. Additionally, their configurations are depicted in Figure 1. The (COD)Ni(dppb) intermediate $\mathbf{I_0}$ is generated through a ligand exchange reaction with dppb, and its relative energy is set to a relative zero value. At the beginning of the reaction, the combination order of HCN and butadiene is considered. When HCN firstly combines with a nickel atom, HCN replacing the other COD in $\mathbf{I_0}$ leads to intermediate $\mathbf{I_1}$ in an exothermic process. The relative energy of intermediate $\mathbf{I_1}$ is −9.6 kcal/mol, which is lower than that of the intermediate formed by butadiene via the same process (−6.8 kcal/mol) (see Appendices A and B). Therefore, the former pathway is selected, as it is thermodynamically favorable.

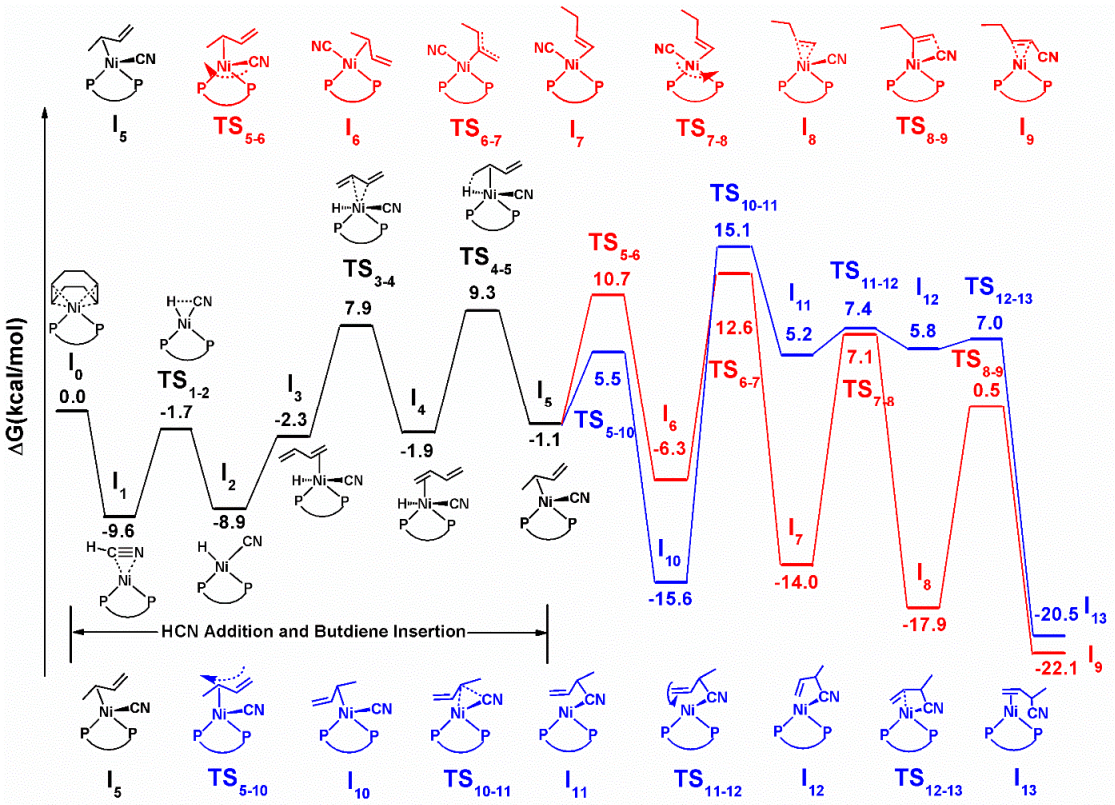

Scheme 5. Detailed mechanism of hydrocyanation using Ni-dppb complex as a catalyst.

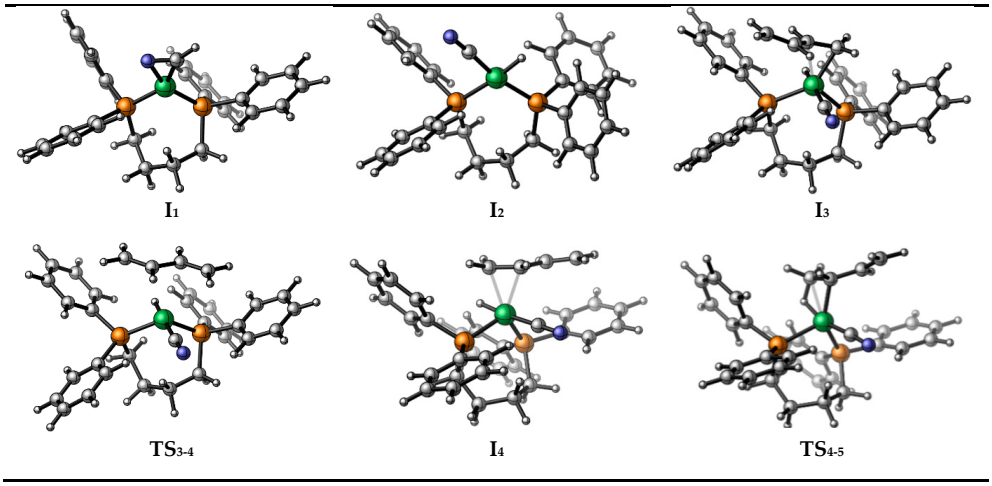

Figure 1. Intermediates and transition states appear in HCN addition and butadiene insertion.

Then, the oxidative addition of HCN forming hydrido nickel cyanide complex (intermediate $\mathbf{I_2}$) takes place and the relative free energy of transition state $\mathbf{TS_{1\text{-}2}}$ is only −1.7 kcal/mol. Next, direct coordination of butadiene occurs to form olefin-coordinated cyano nickel hydride intermediate $\mathbf{I_3}$, here, the coordination mainly refers to the bonding of butadiene via its C=C bond. Since the butadiene molecule has two terminal double bonds, it is possible for nickel to coordinate to either C=C bond to form the olefin complex. Both of the coordination modes ($\mathbf{I_3}$ and $\mathbf{I_4}$) and their transition state ($\mathbf{TS_{3\text{-}4}}$) are considered, as shown in Scheme 5. From the DFT calculation results, the coordination preference is explained by the relative energies of the species that is formed upon bonding the substrate to the nickel atom. Despite the small difference (within 0.4 kcal/mol) between the relative energies of $\mathbf{I_3}$ and $\mathbf{I_4}$, the configuration corresponding to a lower relative energy ($\mathbf{I_4}$) is selected for subsequent reactions. After the intermediate $\mathbf{I_4}$ is formed, a following olefin insertion into the Ni-H bond takes place via transition state $\mathbf{TS_{4\text{-}5}}$ to form methylallyl-coordinated nickel intermediate $\mathbf{I_5}$, with a barrier of 9.3 kcal/mol. Starting from $\mathbf{I_5}$, two different reaction pathways to generate 3PN and 2M3BN, respectively, are proposed. The following elementary steps in the proposed mechanism have been depicted in Scheme 5.

2.2. Mechanism of the Formation of 3PN

As shown in Scheme 5 (red line), after intermediate $\mathbf{I_5}$ is formed, subsequent CN migration occurs via transition state $\mathbf{TS_{5\text{-}6}}$, with a barrier of only 10.7 kcal/mol, to afford quadrilateral intermediate $\mathbf{I_6}$. Then, the methylallyl rearrangement from an internal carbon coordination to a terminal carbon coordination takes place via transition state $\mathbf{TS_{6\text{-}7}}$ to generate intermediate $\mathbf{I_7}$. The relative free energy of that transition state is 12.6 kcal/mol, which is the highest value in the whole reaction pathway. Therefore, the methylallyl rearrangement is the rate-determining step in the formation of 3PN. Next, the CN group migrates to its initial location, and simultaneously, the C=C of the methylallyl combines with nickel via transition state $\mathbf{TS_{7\text{-}8}}$, with a barrier of only 7.1 kcal/mol. Finally, a reductive elimination via transition state $\mathbf{TS_{8\text{-}9}}$ affords intermediate $\mathbf{I_9}$, which subsequently gives the product 3PN.

2.3. Mechanism of the Formation of 2M3BN

Moreover, we have performed calculations for another pathway, which also starts from intermediate $\mathbf{I_5}$. As shown in Scheme 5 (blue line), $\mathbf{I_5}$ can also undergo a pathway followed by the rotation of methylallyl to finally generate the branched product 2M2BN. The detailed pathway is described as follows. The transition state $\mathbf{TS_{5\text{-}10}}$ connects the $\mathbf{I_5}$ to the $\mathbf{I_{10}}$ and lies at 5.5 kcal/mol, which is lower in energy than $\mathbf{TS_{5\text{-}6}}$. This shows that the rotation of methylallyl is favored over the CN migration, with a barrier which is 10.7 kcal/mol. In $\mathbf{I_{10}}$, the nickel coordination site has

a pseudo-tetrahedral geometry, coordinating to both phosphorus atoms in dppb, the methylallyl group and the CN group. Following the rotation, another transition state, $\mathbf{TS_{10\text{-}11}}$, is obtained. Actually, it is the reductive elimination step that subsequently forms 2M3BN. Then, the configuration of intermediate $\mathbf{I_{11}}$ changes to intermediate $\mathbf{I_{12}}$ via the C-C bond rotation with an unexpectedly low barrier. Finally, the coordination of the formed 2M3BN via its C=C bond with Ni atom, replacing its C=N coordination, affords a more stable intermediate $\mathbf{I_{13}}$. In addition, 2M3BN can be directly generated via the reductive elimination of intermediate $\mathbf{I_6}$ and forming a C-CN bond. However, the relative free energy for this transition state is as high at 27.1 kcal/mol (see Appendices A and B). Therefore, this pathway is ruled out. Furthermore, the relative free energy of the rate determining step ($\mathbf{TS_{5\text{-}10}}$) is 15.1 kcal/mol. Compared with the highest relative free energy in the pathway for forming 3PN, the computational results show that the generation of 2M3BN is unfavorable kinetically. It is worth mentioning that the experimental results show that the molar ratio of 3PN to 2M3BN in the hydrocyanation as 97:3, while our computational results reveal that the relative energy difference between the two rate determining steps during the reaction is only 2.5 kcal/mol. The unequal relationship between the reaction rate and the energy barrier indicates that the isomerization of 2M3BN occurs in the reaction system.

2.4. Isomerization of 2M3BN to 3PN

The catalytic isomerization of 2M3BN, a model reaction in the DuPont process, has been performed using $Ni(COD)_2$ and dppb as a catalyst. The best result has been obtained, with 2M3BN reaching a conversion rate of 93.4%, and the selectivity to 3PN is excellent with 99% at 1 h [23]. To the best of our knowledge, the selectivity to 3PN is the highest for the isomerization of 2M3BN. This result inspires us to believe that there could be an isomerization reaction in the process of butadiene hydrocyanation, that is, the generated branched 2M3BN is rapidly isomerized to linear 3PN under the same catalytic system, thus making 3PN the main product of the hydrocyanation.

2.5. Key Intermediate $\boldsymbol{I_5}$

As mentioned above, there are two reaction pathways (the CN migration and the methylallyl rotation) starting from intermediate $\mathbf{I_5}$, which correspond to the production of 3PN and 2M3BN. Therefore, intermediate $\mathbf{I_5}$ can be regarded as a key intermediate. The bite angle (β) is a key parameter for evaluating the steric effect of a phosphorus ligand. In order to further explain the two pathways, the configurations of intermediates and transition states after intermediate $\mathbf{I_5}$ are studied, and their bite angles are shown in Figure 2. The β of the intermediates and transition states in the pathway to the product 3PN (red line) is significantly smaller than that of the intermediates or transition states appearing in the pathway to generate 2M3BN (blue line). In addition, the configurations of intermediates and transition states are quadrilateral in the pathway of forming 3PN, such as intermediate $\mathbf{I_6}$ (Figure 3) and transition state $\mathbf{TS_{6\text{-}7}}$, which is the reason why their bite angles are close to 90°. In the pathway for the formation of 2M3BN, pseudo-tetrahedral configurations of the intermediates and transition states are found, such as intermediate $\mathbf{I_{10}}$ (Figure 3) and transition state $\mathbf{TS_{10\text{-}11}}$, which correspond to larger bite angle. Therefore, using dppb as a ligand, the effect of bridge moiety in the ligand skeleton on the catalytic pathway is revealed. The bite angles of the intermediates or transition states with flexible ligand skeletons are varied during the catalytic reaction instead of maintaining it in a small range. Different bite angles make the reaction proceed in different and reasonable directions.

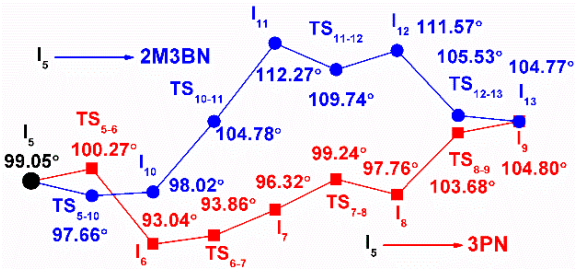

Figure 2. The bite angle of the intermediates and transition states.

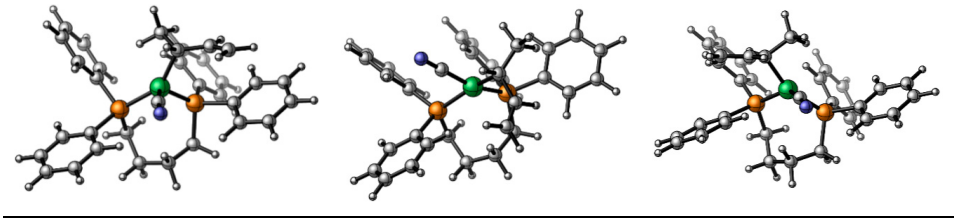

Figure 3. The structure of the three intermediates ($\mathbf{I_5}$, $\mathbf{I_6}$ and $\mathbf{I_{10}}$).

3. Materials and Methods

All of the DFT calculations conducted in this study were carried out using the Gaussian 09 series of programs [24]. Firstly, To determine the right density functional, we optimized the geometry of the intermediate Ni(η^3-1-Me-C_3H_4)(CN)(dppb) complex [21] using B3LYP, B3LYP(D3), M06-2X, M11-L and ωB97XD, based on its crystal data. Density functional M11-L [25], proposed by Truhlar et al., with a standard 6-31G(d) [26,27] basis set (SDD [28] basis set for Ni), could provide great accuracy in energy information for its most realistic description of the geometry of the intermediate, which was the foundation of gaining proper free energy and vibration analysis [23]. In the calculation, all molecules have charges of zero and spin multiplicities of one (Charge = 0, Multiplicity = 1). Harmonic vibrational frequency calculations were performed for all stationary points to confirm them as local minima or transition structures and to derive the thermochemical corrections for the enthalpies and free energies. The same DFT method was used with a 6-311G+(d, p) basis set [29–31] (SDD basis set for Ni) to calculate the single-point energies. Solvent effects were taken into consideration using single-point calculations based on the gas-phase stationary points with a SMD continuum solvation model [32]. The energies presented in this paper are the M11-L/6-311+G(d, p) calculated Gibbs free energies in cumene [33], with M11-L/6-31G(d) calculated thermodynamic corrections. The CYLview [34] was employed to represent the intermediates. In addition, atomic coordinates of intermediates and transition states are provided in Supplementary Materials (Table S1).

4. Conclusions

In the DuPont process for hydrocyanation of butadiene, the reaction mechanism using a nickel complex with a mono-dentate phosphorus ligand as the catalyst has been reported; however, reports on research using a diphosphine ligand, especially the reaction mechanism, are limited. In this paper, a reasonable reaction mechanism of the hydrocyanation is proposed, and the key intermediate and the rate-determining steps in the reaction have been illustrated. For the hydrocyanation reaction of butadiene using Ni(dppb), the mechanism involving the CN migration (for 3PN) and the methylallyl rotation (for 2M3BN) pathways have been proposed based on DFT calculations. $\mathbf{I_5}$ is the key intermediate for there are two changes in its configuration. In the following pathways, the methylallyl rearrangement is the rate determining step in the formation of 3PN while the reductive elimination governs the reaction to 2M3BN, which is subsequently isomerized to 3PN. Further research shows

that in the above two reaction pathways, the bite angle of the intermediates and transition states has the opposite trend due to the flexibility of the dppb ligand skeleton. Therefore, the selectivity of the reaction can be controlled by changing the rigidity of the ligand backbone.

Supplementary Materials: The following are available online at http://www.mdpi.com/2073-4344/10/8/818/s1, Table S1: Atomic coordinates of the intermediates and transition states.

Author Contributions: Conceptualization, methodology, software, validation, investigation, resources, data curation, writing—original draft preparation, writing—review and editing, and visualization, K.L.; supervision and project administration, S.Z.; funding acquisition, M.H. All authors have read and agreed to the published version of the manuscript.

Funding: This research received no external funding.

Acknowledgments: We thank Chen Tao (Anhui Shuguang Chemical Group) for providing us with technical guidance and experimental assistance.

Conflicts of Interest: The authors declare no conflict of interest.

Appendix A

Here, the direct combination of butadiene and the catalyst is considered, and its structure is shown in Figure A1 in Appendix B, the corresponding energy is −6.8 kcal/mol.

While dppb replaces the COD in $\mathbf{I_0}$ to form the bis-chelate intermediate (Ni(dppb)$_2$) (see Figure A1 in Appendix B), with a relative energy of 7.31 kcal/mol. Compared with the relative energy of intermediate $\mathbf{I_1}$ (−9.6 kcal/mol), the generation of Ni(dppb)$_2$ is thermodynamically unfavorable.

In addition, to form 2M3BN, the directly forming C-CN bond via reductive elimination of intermediate I_6 is another pathway. Its structure is depicted in Figure A1. However, the relative free energy of this transition state is as high as 27.1 kcal/mol. Therefore, this pathway is ruled out.

Appendix B

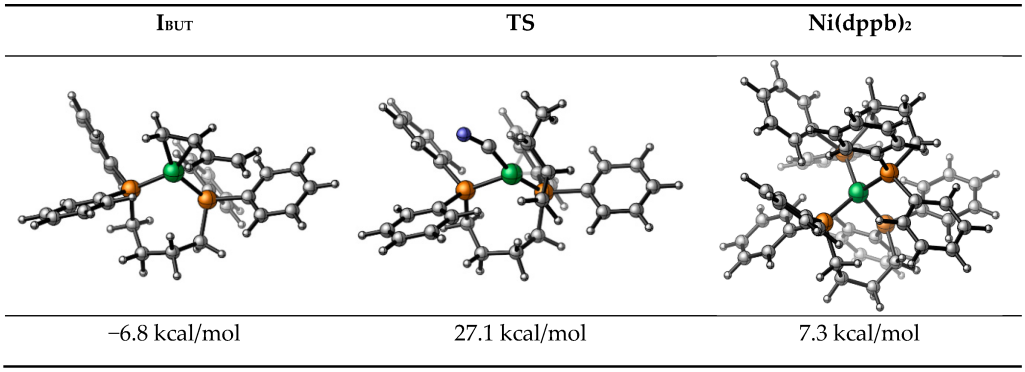

Figure A1. The structure of the intermediate I_{BUT}, transition state **TS** and Ni(dppb)$_2$.

References

1. Gillespie, J.A.; Zuidema, E.; van Leeuwen, P.W.N.M.; Kamer, P.C.J. *Phosphorus(III) Ligands in Homogeneous Catalysis: Design and Synthesis*, 1st ed.; Wiley: John Wiley & Sons, Ltd: Chichester, UK, 2012; pp. 1–26. [CrossRef]
2. Vogt, D.; Wilting, J. Reduction: Hydrocyanation of C=C. In *Comprehensive Chirality*; Carreira, E.M., Yamamoto, H., Eds.; Elsevier: Amsterdam, The Netherlands, 2012; pp. 343–354. [CrossRef]
3. RajanBabu, T.V. *Hydrocyanation in Organic Synthesis, in Comprehensive Organic Synthesis II*, 2nd ed.; Knochel, P., Ed.; Elsevier: Amsterdam, The Netherlands, 2014; pp. 1772–1793. [CrossRef]
4. Seidel, W.C.; Tolman, C.A. Homogeneous nickel-catalyzed olefin hydrocyanation. *Annal. N. Y. Acad. Sci.* **1983**, *415*, 201–221. [CrossRef]

5. Tolman, C.A.; Seidel, W.C.; Gosser, L.W. Formation of three-coordinate nickel(0) complexes by phosphorus ligand dissociation from NiL_4. *J. Am. Chem. Soc.* **1974**, *96*, 53–60. [CrossRef]
6. Tolman, C.A.; McKinney, R.J.; Seidel, W.C.; Druliner, J.D.; Stevens, W.R. Homogeneous Nickel-Catalyzed Olefin Hydrocyanation. *Adv. Catal.* **1985**, *33*, 1–46. [CrossRef]
7. Baker, M.J.; Pringle, P.G. Chiral aryl diphosphites: A new class of ligands for hydrocyanation catalysis. *J. Chem. Soc. Chem. Commun.* **1991**, *18*, 1292–1293. [CrossRef]
8. Tolman, C.A. Electron donor-acceptor properties of phosphorus ligands. Substituent additivity. *J. Am. Chem. Soc.* **1970**, *92*, 2953–2956. [CrossRef]
9. Tolman, C.A. Phosphorus ligand exchange equilibriums on zerovalent nickel. Dominant role for steric effects. *J. Am. Chem. Soc.* **1970**, *92*, 2956–2965. [CrossRef]
10. Tolman, C.A. The 16 and 18 electron rule in organometallic chemistry and homogeneous catalysis. *Chem. Soc. Rev.* **1972**, *1*, 337–353. [CrossRef]
11. Tolman, C.A. Steric effects of phosphorus ligands in organometallic chemistry and homogeneous catalysis. *Chem. Rev.* **1977**, *77*, 313–348. [CrossRef]
12. Van der Vlugt, J.I.; Hewat, A.C.; Neto, S.; Sablong, R.; Mills, A.M.; Lutz, M.; Spek, A.L.; Müller, C.; Vogt, D. Sterically Demanding Diphosphonite Ligands-Synthesis and Application in Nickel-Catalyzed Isomerization of 2-Methyl-3-Butenenitrile. *Adv. Synth. Catal.* **2004**, *346*, 993–1003. [CrossRef]
13. Wilting, J.; Müller, C.; Hewat, A.C.; Ellis, D.D.; Tooke, D.M.; Spek, A.L.; Vogt, D. Nickel-Catalyzed Isomerization of 2-Methyl-3-butenenitrile. *Organometallics* **2005**, *24*, 13–15. [CrossRef]
14. Bini, L.; Müller, C.; Vogt, D. Mechanistic Studies on Hydrocyanation Reactions. *ChemCatChem* **2010**, *2*, 590–608. [CrossRef]
15. Bini, L.; Müller, C.; Vogt, D. Ligand development in the Ni-catalyzed hydrocyanation of alkenes. *Chem. Commun.* **2010**, *46*, 8325–8334. [CrossRef] [PubMed]
16. García, J.J.; Arévalo, A.; Brunkan, N.M.; Jones, W.D. Cleavage of Carbon-Carbon Bonds in Alkyl Cyanides Using Nickel(0). *Organometallics* **2004**, *23*, 3997–4002. [CrossRef]
17. Acosta-Ramírez, A.; Flores-Gaspar, A.; Muñoz-Hernández, M.; Arévalo, A.; Jones, W.D.; García, J.J. Nickel Complexes Involved in the Isomerization of 2-Methyl-3-butenenitrile. *Organometallics* **2007**, *26*, 1712–1720. [CrossRef]
18. Swartz, B.D.; Reinartz, N.M.; Brennessel, W.W.; García, J.J.; Jones, W.D. Solvent Effects and Activation Parameters in the Competitive Cleavage of C-CN and C-H Bonds in 2-Methyl-3-Butenenitrile Using $[(dippe)NiH]_2$. *J. Am. Chem. Soc.* **2008**, *130*, 8548–8554. [CrossRef] [PubMed]
19. Li, T.; Jones, W.D. DFT Calculations of the Isomerization of 2-Methyl-3-butenenitrile by [Ni(bisphosphine)] in Relation to the DuPont Adiponitrile Process. *Organometallics* **2011**, *30*, 547–555. [CrossRef]
20. Tolman, C.A.; Seidel, W.C.; Druliner, J.D.; Domaille, P.J. Catalytic hydrocyanation of olefins by nickel(0) phosphite complexes-effects of Lewis acids. *Organometallics* **1984**, *3*, 33–38. [CrossRef]
21. Chaumonnot, A.; Lamy, F.; Sabo-Etienne, S.; Donnadieu, B.; Chaudret, B.; Barthelat, J.-C.; Galland, J.-C. Catalytic Isomerization of Cyanoolefins Involved in the Adiponitrile Process. C-CN Bond Cleavage and Structure of the Nickel π-Allyl Cyanide Complex $Ni(\eta^3\text{-}1\text{-}Me\text{-}C_3H_4)(CN)(dppb)$. *Organometallics* **2004**, *23*, 3363–3365. [CrossRef]
22. Liu, K.; Liu, K.-K.; Cheng, M.-J.; Han, M.-H. Theoretical and experimental study of the nickel-catalyzed isomerization of 2-Methyl-3-butenenitrile and the effect of a Lewis acid. *J. Organomet. Chem.* **2016**, *822*, 29–38. [CrossRef]
23. Liu, K.; Xin, H.; Han, M. Elucidation of key factors in nickel-diphosphines catalyzed isomerization of 2-methyl-3-butenenitrile. *J. Catal.* **2019**, *377*, 13–19. [CrossRef]
24. Frisch, M.J.; Trucks, G.W.; Schlegel, H.B.; Scuseria, G.E.; Robb, M.A.; Cheeseman, J.R.; Scalmani, G.; Barone, V.; Mennucci, B.; Petersson, G.; et al. *Gaussian 09, Revision E.01*; Gaussian, Inc.: Wallingford, CT, USA, 2015.
25. Peverati, R.; Truhlar, D.G. M11-L: A Local Density Functional That Provides Improved Accuracy for Electronic Structure Calculations in Chemistry and Physics. *J. Phys. Chem. Let.* **2012**, *3*, 117–124. [CrossRef]
26. Hariharan, P.C.; Pople, J.A.J.T.C.A. The influence of polarization functions on molecular orbital hydrogenation energies. *Theor. Chim. Acta* **1973**, *28*, 213–222. [CrossRef]
27. Francl, M.M.; Pietro, W.J.; Hehre, W.J.; Binkley, J.S.; Gordon, M.S.; Defrees, D.J.; Pople, J.A. Self-consistent Molecular-orbital Methods. XXIII. A Polarization-type Basis Set For 2nd-row Elements. *J. Chem. Phys.* **1982**, *77*, 3654–3665. [CrossRef]

28. Dolg, M.; Wedig, U.; Stoll, H.; Preuss, H. Energy adjusted ab initio pseudopotentials for the first row transition elements. *J. Chem. Phys.* **1987**, *86*, 866–872. [CrossRef]
29. Krishnan, R.; Binkley, J.S.; Seeger, R.; Pople, J.A. Self-consistent molecular orbital methods. XX. A basis set for correlated wave functions. *J. Chem. Phys.* **1980**, *72*, 650–654. [CrossRef]
30. McLean, A.D.; Chandler, G.S. Contracted Gaussian basis sets for molecular calculations. I. Second row atoms, Z=11-18. *J. Chem. Phys.* **1980**, *72*, 5639–5648. [CrossRef]
31. Blaudeau, J.-P.; McGrath, M.P.; Curtiss, L.A.; Radom, L. Extension of Gaussian-2 (G2) theory to molecules containing third-row atoms K and Ca. *J. Chem. Phys.* **1997**, *107*, 5016–5021. [CrossRef]
32. Marenich, A.V.; Cramer, C.J.; Truhlar, D.G. Performance of SM6, SM8, and SMD on the SAMPL1 Test Set for the Prediction of Small-Molecule Solvation Free Energies. *J. Phys. Chem. B.* **2009**, *113*, 4538–4543. [CrossRef]
33. Liu, K.; Han, M. Solvent-Controlled the Isomerization of 2-Methyl-3-Butenenitrile. *Molecules*. under review.
34. Legault, C.Y. CYLview. 2009, Université de Sherbrooke. Available online: http://www.cylview.org (accessed on 11 February 2018).